SCIENTIFIC REPORTS

OPEN

SUBJECT AREAS:
BATTERIES
SYNTHESIS AND PROCESSING

Received
1 September 2014

Accepted
11 November 2014

Published
5 December 2014

Correspondence and requests for materials should be addressed to K.P. (park@austin.utexas.edu) or I-D.K. (idkim@kaist.ac.kr)

Multi-layer electrode with nano-$Li_4Ti_5O_{12}$ aggregates sandwiched between carbon nanotube and graphene networks for high power Li-ion batteries

Jin-Hoon Choi[1,4,5], Won-Hee Ryu[1], Kyusung Park[2], Jeong-Dai Jo[3], Sung-Moo Jo[4], Dae-Soon Lim[5] & Il-Doo Kim[1]

[1]Department of Materials Science & Engineering, Korea Advanced Institute of Science & Technology, 335 Science Road, Daejeon 305-701, Republic of Korea, [2]Texas Materials Institute, The University of Texas at Austin, Austin, Texas 78712, United States, [3]Intelligence and Precision Machinery Research Division, Korea Institute of Machinery and Materials, Daejeon, 305-343, Republic of Korea, [4]Carbon Convergence Materials Research Division, Korea Institute of Science and Technology, Seoul 136-791, Republic of Korea, [5]Department of Materials Science and Engineering, Korea University, Seoul 136-713, Republic of Korea.

Self-aggregated $Li_4Ti_5O_{12}$ particles sandwiched between graphene nanosheets (GNSs) and single-walled carbon nanotubes (SWCNTs) network are reported as new hybrid electrodes for high power Li-ion batteries. The multi-layer electrodes are fabricated by sequential process comprising air-spray coating of GNSs layer and the following electrostatic spray (E-spray) coating of well-dispersed colloidal $Li_4Ti_5O_{12}$ nanoparticles, and subsequent air-spray coating of SWCNTs layer once again. In multi-stacked electrodes of GNSs/nanoporous $Li_4Ti_5O_{12}$ aggregates/SWCNTs networks, GNSs and SWCNTs serve as conducting bridges, effectively interweaving the nanoporous $Li_4Ti_5O_{12}$ aggregates, and help achieve superior rate capability as well as improved mechanical stability of the composite electrode by holding $Li_4Ti_5O_{12}$ tightly without a binder. The multi-stacked electrodes deliver a specific capacity that maintains an impressively high capacity of 100 mA h g^{-1} at a high rate of 100C even after 1000 cycles.

Emerging interests in large-scale energy storage for hybrid electric vehicles and smart grids[1–3] and in high-capacity flexible batteries[4–7] have inspired research efforts to develop rechargeable lithium-ion batteries (LIBs) with high power and high energy density. Novel electrode designs and optimized synthetic methods for advanced LIBs have been suggested to open up diverse applications. The conventional electrode structure fabricated by the slurry casting route often induces a substantial loss in electrical contacts especially if the size of the active material is in the nano-scale[8]. Moreover, for utilizing nano-sized electrode materials, the loading level of the polymeric binder that holds both active materials and carbon additives together must be further increased, which is detrimental to the electrode energy density. Therefore, developing binder-free electrode architectures with optimal electrical connections could be an essential solution to not only maximize the energy density but also to guarantee the high power capability, while the mechanical stability of the electrode should also be assured for long-term durability. Until now, several approaches have been proposed to fabricate binder-free electrodes such as the spray-coating of Si nanowire-based ink on the carbon textiles matrix[7], uniform loading of SnO_2 nanoparticles onto cross-stacked carbon nanotube (CNT) sheets[9], forming nanostructured MnO_2 monolith on the cotton texture template by post heat treatment[10], dispersing CNT using the electrostatic spray (E-spray) method[11] and fabrication of a $LiFePO_4$/conducting polymer composite[12]. In this work, $Li_4Ti_5O_{12}$ anode material was chosen to verify the feasibility of the binder-free electrode concept fabricated via controlled aggregation of $Li_4Ti_5O_{12}$ nanoparticles and the subsequent wrapping with carbon networks.

Lithium titanate, $Li_4Ti_5O_{12}$ has received great attention due to its outstanding structural stability during electrochemical cycling, excellent coulombic efficiency due to the stable $Li_4Ti_5O_{12}$/electrolyte interface, and the fast electrode kinetics enhanced by the 3-dimensional Li^+-ion diffusion pathways in the spinel structure. However, the low theoretical capacity (175 mA h g^{-1}) of $Li_4Ti_5O_{12}$ has been considered as one of the intrinsic limitations along with its high charge/discharge voltage of around 1.5 V vs. Li^+/Li[13–18]. Recently, Park et al. proposed a carbon-free $Li_4Ti_5O_{12}$ electrode concept, which showed a fast-growing, electrically-conductive

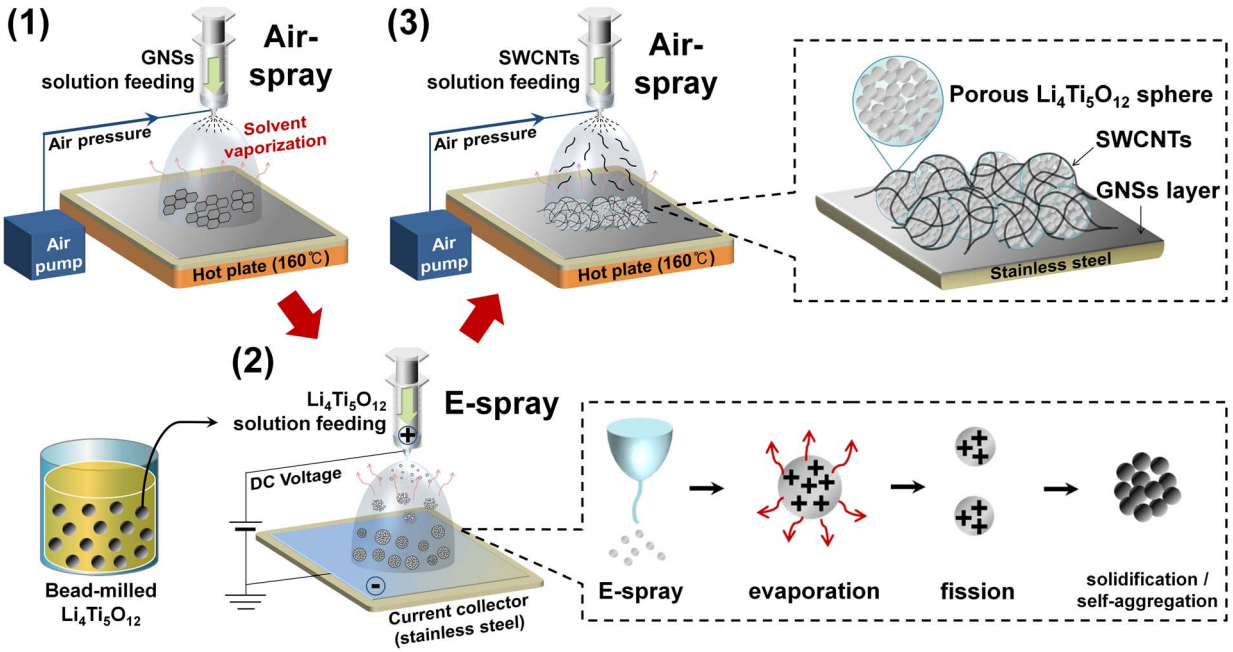

Figure 1 | Schematic illustration of sequential fabrication steps for the multi-stacked GNSs/$Li_4Ti_5O_{12}$/SWCNTs electrode consisting of the self-aggregated nanoporous $Li_4Ti_5O_{12}$ interconnected by GNSs and SWCNTs.

$Li_{4+\alpha}Ti_5O_{12}$ surface phase at a low lithiation state[19]. Exclusion of the carbon and minimal use of the polymer binder in the electrode maximized the electrode energy density. The work has been quickly revisited and validated by Cabana et al[20]. They also emphasized the importance of physical inter-particle contacts, especially if the active material becomes nano-sized. For the nano-$Li_4Ti_5O_{12}$ with high surface area and poor inter-particle contacts, the propagation of the conductive $Li_{4+\alpha}Ti_5O_{12}$ surface phase should be kinetically limited. The idea supports the fact that the previous works on nano-$Li_4Ti_5O_{12}$ have been particularly focused on the surface coating of $Li_4Ti_5O_{12}$ with conductive materials such as carbon and nitrides[21,22]. This motivated us to design a new electrode architecture using $Li_4Ti_5O_{12}$ nanoparticles. We promoted good physical contacts between the nano-$Li_4Ti_5O_{12}$ particles by making compact aggregates but limited the aggregate sizes to ensure the fast propagation of the surface conducting phase during Li insertion/extraction cycles. The aggregates were further wrapped with a minimal amount (<3 wt.%) of carbon to realize the binder-free electrode.

In this work, we used the E-spray coating method to form spherical $Li_4Ti_5O_{12}$ aggregates with compact inter-particle contacts between the nano-$Li_4Ti_5O_{12}$ primary particles. The spray process enables the direct coating of pre-synthesized colloidal particles on the current collector without any conductive carbon black and binder[23–26]. In particular, it also provides porous 3-dimensional secondary particle structures without the use of hard templates. The aggregation could increase the tap density and the volumetric energy density as well[27–29].

Afterward, the electrical wiring of the secondary particles was achieved by carbon wrapping, which was necessary because it could greatly reduce the effective electron migration path in the electrode, as evidenced by the previous work on thin and thick $Li_4Ti_5O_{12}$ electrodes[20]. The graphene nanosheets (GNSs) and single-walled carbon nanotubes (SWCNTs) networks can efficiently provide the electrical currents to $Li_4Ti_5O_{12}$ particles from the current collector and increase the mechanical stability of the electrode by interweaving the electrode components. Their outstanding electrical conductivity (in the case of a graphene sheet: 2×10^5 cm^2 V^{-1} S^{-1})[30], ultrathin nature, good structural flexibility and high mechanical strength (Young's modulus of SWCNT and GNS: ~1 TPa)[31,32] are crucial to the efficiency and stability improvements of the hybrid electrode[33–37]. The multi-stacked GNSs/$Li_4Ti_5O_{12}$/SWCNTs structure showed superior electrode energy density and kinetic properties during long-term cycling (1000 cycles), even at 100 C-rate.

Results

A sandwich-type hybrid electrode employing carbon-free $Li_4Ti_5O_{12}$ aggregates was prepared by multiple spray depositions, as illustrated in Figure 1. The sequential steps include a series of (1) air-spray deposition of GNSs as an intermediate buffer layer on a stainless steel current collector and (2) electrostatic spraying of the colloidal nano-$Li_4Ti_5O_{12}$ powder pulverized by high energy micro-bead milling (Supplementary Fig. S1)[38]. The close-packed particle structure of the $Li_4Ti_5O_{12}$ aggregates was obtained through the evaporation of the ethanol solvent with a low boiling point (78.37°C) and the solidification after the fission droplet process as illustrated in the inset image (bottom right). The last step is (3) air-spray deposition of SWCNTs to interconnect and wrap the $Li_4Ti_5O_{12}$ aggregates stacked on GNSs. Finally, the spherical $Li_4Ti_5O_{12}$ secondary particles could be wrapped and interconnected between GNSs and SWCNTs as illustrated in the inset (top right) of Figure 1. For electrochemical cell tests, the electrodes have been fabricated with different loading levels by repeating the sequential steps described above. The processes of (2) and (3) have been repeated three times (G-3 layer LTO-C), six times (G-6 layer LTO-C), and nine times (G-9 layer LTO-C), respectively.

In the series of the deposition processes to form the multi-stacked GNSs/$Li_4Ti_5O_{12}$/SWCNTs electrodes, an important prerequisite is preparing uniform $Li_4Ti_5O_{12}$ nano-particles and nano-suspensions for the electrostatic and air spray coatings. In this work, GNSs and SWCNTs were used as received, but $Li_4Ti_5O_{12}$ was micro-bead milled using 0.1 mm ZrO_2 balls to obtain uniformly dispersed $Li_4Ti_5O_{12}$ colloidal particles in ethanol. We optimized the milling time to control the particle size and distribution. The X-ray diffraction pattern of the pristine $Li_4Ti_5O_{12}$ was indexed to be a cubic spinel structure (space group: $Fd\bar{3}m$, JCPDS No. 49-0207) without any impurity phases (Supplementary Fig. S2a). With increasing the bead-milling time, the diffraction peaks broadened as a result of the reduced crystallite size corresponding to the Scherrer equation,

$\tau = K\lambda/\beta\cos\theta$, where τ is the mean size of the crystalline particles, K is the shape factor, λ is the X-ray wavelength, β is the line broadening at full width at half maximum (FWHM) in radians, and θ is the Bragg angle. The crystallite sizes of the bead-milled $Li_4Ti_5O_{12}$ were estimated from the equation to be 33, 26 and 21 nm after milling the powder for 20, 40 and 60 minutes, respectively (Supplementary Fig. S2b). The result was also confirmed by transmission electron microscopy (TEM) analysis (Supplementary Fig. S3). The $Li_4Ti_5O_{12}$ nanoparticles with the crystallite size of 21 nm were selected to make a colloidal solution for the electrostatic spray coating process.

Figure 2 shows the microstructural evolution of the self-aggregated carbon-free $Li_4Ti_5O_{12}$ secondary particles (Figure 2a). We identified that the individual nano-particles obtained via the micro-bead milling have a crystalline $Li_4Ti_5O_{12}$ phase with a d-spacing of 0.48 nm for (111) plane, as indicated in a high-resolution TEM image (Figure 2f). Moreover, even though all electron diffraction ring patterns were blurred due to the nano-size effect, they could be indexed as the spinel $Li_4Ti_5O_{12}$ phase, which is in good agreement with the X-ray diffraction (XRD) results of the bead-milled $Li_4Ti_5O_{12}$ powders (see Figure 2b and Supplementary Fig. S2a). After the E-spray coating, the $Li_4Ti_5O_{12}$ nanoparticles were aggregated to a spherical shape (Figure 2c and 2d). The sizes of secondary spherical particles ranged from 300 to 700 nm and the average size was approximately 500 nm. Figure 2e is a magnified TEM image of the aggregated $Li_4Ti_5O_{12}$ spherical particle, which shows that it was composed of tightly packed primary particles ranging from 20 to 30 nm. In addition, a significant amount of interconnected nanopores was also observed, which is important for electrolyte wetting and Li^+-ion feeding. A high specific BET surface area of 54 $m^2\ g^{-1}$ was confirmed in the $Li_4Ti_5O_{12}$ aggregates. With the E-spray process, we were able to control the size of the carbon-free $Li_4Ti_5O_{12}$ aggregates to be small enough to reproduce a thin electrode case[19,20].

Figure 3 shows the morphology of the GNSs/$Li_4Ti_5O_{12}$/SWCNTs hybrid electrodes. The nanoporous $Li_4Ti_5O_{12}$ aggregates were effectively wrapped by interwoven SWCNTs networks (Figure 3a and 3b). In addition, SWCNTs were found to be connected to GNSs deposited onto the stainless steel substrate (yellow circles in Figure 3c and 3d). Figure 3a–f show uniform and effective networking among the GNSs, SWCNTs, and $Li_4Ti_5O_{12}$. SWCNTs wrapping the spherical $Li_4Ti_5O_{12}$ particles provide both facile electron pathways and help to tightly bind the $Li_4Ti_5O_{12}$ aggregates. The GNSs/$Li_4Ti_5O_{12}$ electrode without SWCNTs showed poor mechanical strength (Supplementary Fig. S4). With this hybrid GNSs/$Li_4Ti_5O_{12}$/SWCNTs structure, we could eliminate the electrically insulating binders such as polyvinylidene fluoride (PVDF) and greatly reduce the electrode impedance; The electrode resistance of the hybrid electrode was much less than that of the GNSs/$Li_4Ti_5O_{12}$ electrode (Supplementary Fig. S5 and S6).

Discussion

The electrochemical properties of the GNSs/$Li_4Ti_5O_{12}$/SWCNTs hybrid electrode were investigated as shown in Figure 4. For comparison, the pristine and bead-milled $Li_4Ti_5O_{12}$ electrodes having 10 wt.% carbon black and 8 wt.% PVDF binder were prepared by the conventional slurry casting method. Table S1 shows loading levels of the $Li_4Ti_5O_{12}$ electrodes with different deposition layers and the corresponding applied current densities at each C-rate.

Figure 4a exhibits the first three charge/discharge voltage curves of the GNSs/$Li_4Ti_5O_{12}$/SWCNTs hybrid electrode. The loading amount of carbon from GNSs and SWCNTs components was mea-

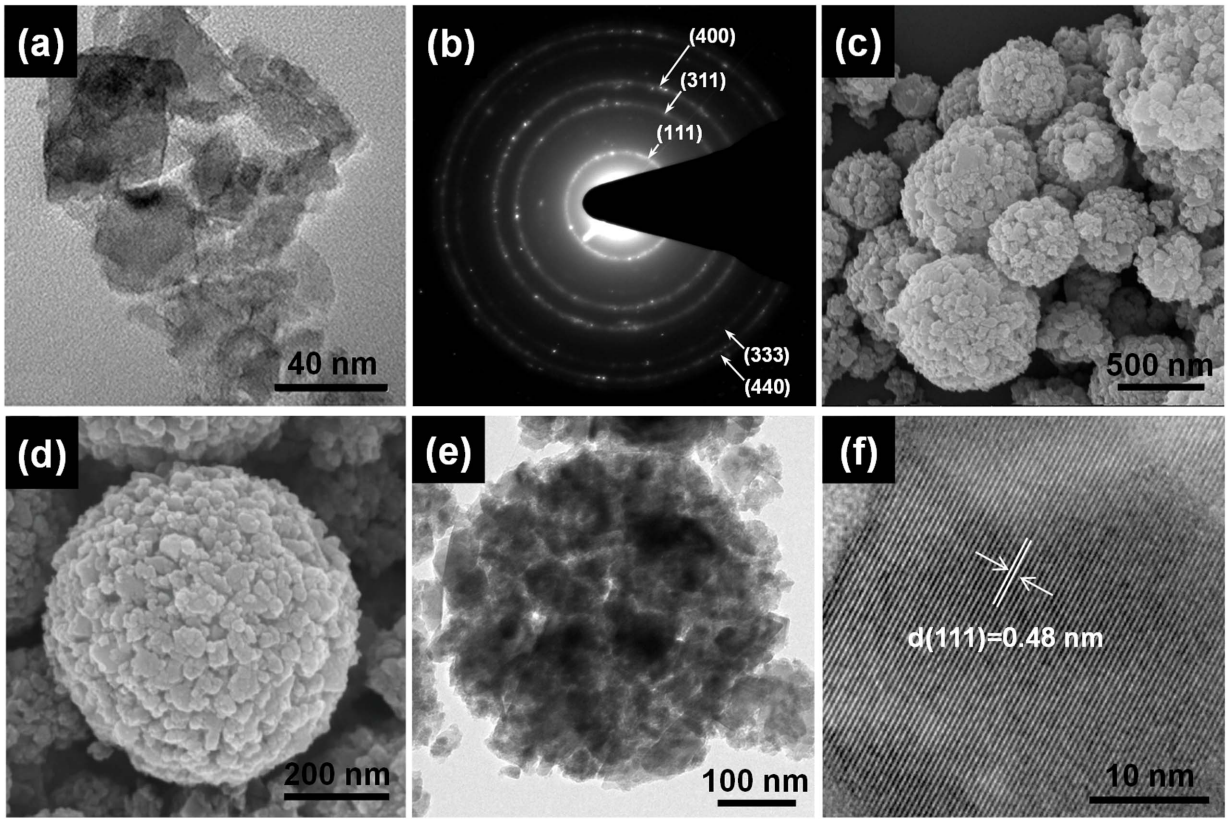

Figure 2 | Microstructure of self-aggregated carbon-free $Li_4Ti_5O_{12}$ spheres. (a) TEM image of the nanosized $Li_4Ti_5O_{12}$ prepared by bead-milling for 60 min, (b) selected area electron diffraction (SAED) pattern of the bead-milled $Li_4Ti_5O_{12}$, (c–d) SEM images and (e) TEM image of the self-aggregated carbon-free $Li_4Ti_5O_{12}$ spheres obtained by E-spray deposition of the bead-milled $Li_4Ti_5O_{12}$, (f) lattice fringes of the nanoparticle comprising the self-aggregated $Li_4Ti_5O_{12}$ spheres.

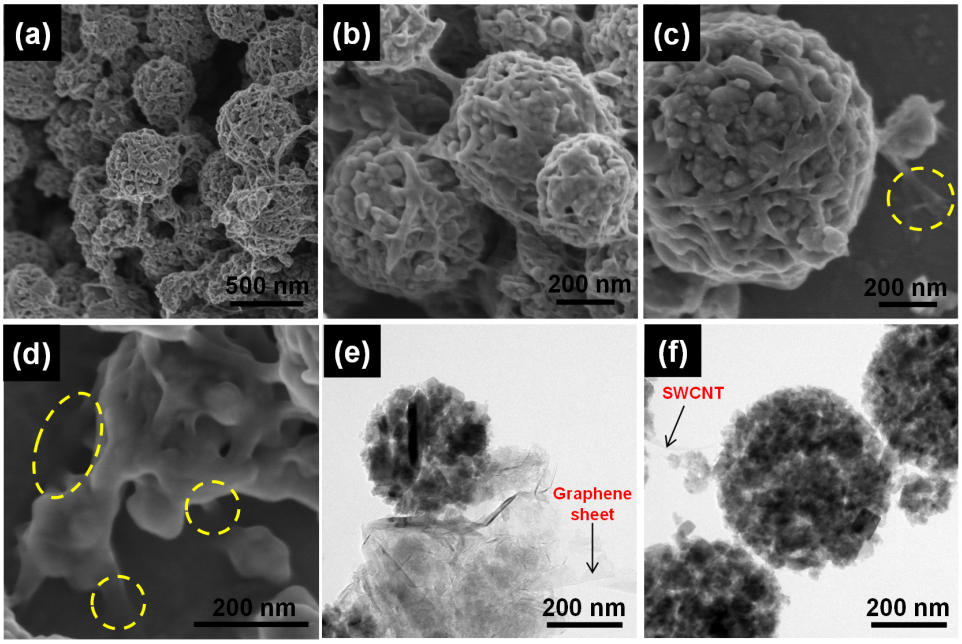

Figure 3 | Microstructure of carbon-networked binder-free $Li_4Ti_5O_{12}$ spheres. (a–c) SEM images and (d–f) TEM images of the self-aggregated nanoporous $Li_4Ti_5O_{12}$ hybrid electrodes interconnected by GNSs and SWCNTs at different magnifications. Yellow circle regions highlight the connections between GNSs and SWCNTs.

sured to be 2.9 wt.%, which is extremely low considering the nano-sized electrode materials. The typical voltage plateaus at ~1.5 V both for charging and discharging were also identified, indicating a two-phase equilibrium reaction between $Li_4Ti_5O_{12}$ and $Li_7Ti_5O_{12}$. However, unlike the charge/discharge characteristics of bulk $Li_4Ti_5O_{12}$, there are sloping voltage curves before and after the voltage plateau. This region can be described as a surface-dominated pseudocapacitive charge/discharge reaction[39]. The other possible origin could be a nano-size effect that can reduce the miscibility gap and increase the solid solution region during an electrochemical reaction, which is well documented in the study of $LiFePO_4$[40]. Regardless of the models stated above, it is highly likely that the surface layer of $Li_4Ti_5O_{12}$ is diffusively lithiated and delithiated in the early charge and discharge reactions before nucleating $Li_7Ti_5O_{12}$ (or $Li_{7-\beta}Ti_5O_{12}$) and $Li_4Ti_5O_{12}$ (or $Li_{4+\alpha}Ti_5O_{12}$), respectively. Since the lithiated lithium concentration is dilute for such a high surface area, coulombic interactions between lithium ions to form the $Li_7Ti_5O_{12}$ domain could also be ignored in this initial stage during discharge. The lithiation-induced $Li_{4+\alpha}Ti_5O_{12}$ phase with high concentration of Ti^{3+} ($3d^1$) at the particle surface can enhance the surface electronic conductivity of $Li_4Ti_5O_{12}$, which was previously proposed in the micron-sized $Li_4Ti_5O_{12}$[19]. We can exclude the possibility of the electrochemical participation from GNSs and SWCNTs because the discharge cut-off voltage was set to 1.0 V, which is higher than the redox voltage of typical carbon species.

Figure 4b shows the discharge capacities of the pristine $Li_4Ti_5O_{12}$ (slurry coating), bead-milled $Li_4Ti_5O_{12}$ (slurry coating), and GNSs/$Li_4Ti_5O_{12}$/SWCNTs electrodes at different current densities; rate capabilities of the GNSs/$Li_4Ti_5O_{12}$/SWCNTs electrodes and the slurry-casted electrodes with different loading densities of 0.45 and 1.3 mg cm^{-2} were also investigated, as shown in Supplementary Fig. S7a and S7b. The average discharge capacity of the GNSs/$Li_4Ti_5O_{12}$/SWCNTs hybrid electrode (148.9 mA h g^{-1} at 1C) is superior to those of the pristine and the bead-milled $Li_4Ti_5O_{12}$ electrodes (144.4 and 145.8 mA h g^{-1}, respectively). Strikingly, the rate capability of the hybrid electrode is excellent while the other two $Li_4Ti_5O_{12}$ electrodes with higher carbon loading content (10 wt.%) show poor electrochemical kinetics. The slurry-casted $Li_4Ti_5O_{12}$ electrodes were unable to sustain C-rates higher than 20C while $Li_4Ti_5O_{12}$ in the hybrid electrode could deliver 109.3 mA h g^{-1} even at 100C. Note that the hybrid electrode contains $Li_4Ti_5O_{12}$ with a very high surface area of 54 $m^2 g^{-1}$ along with carbon content as low as 2.9 wt.%. After the 100 C-rate cycling, the capacity was fully recovered when the current density was reduced back to 1 C-rate, which indicates there was no irreversible electrode degradation during high C-rate cycling. These results confirm the stable electrochemical activity of the $Li_4Ti_5O_{12}$ aggregates composed of carbon-free nanoparticles. The nano-particle aggregation ensures intimate inter-particle contacts while the nanopores can facilitate the Li^+-ion transports to the individual particles. The uniform electrical wiring of the $Li_4Ti_5O_{12}$ spherical particles with GNSs and SWCNTs effectively enhances electronic conduction from the current collector to each aggregate. In addition, unlike the dense and compact electrode structure of the slurry-casted electrode, the hybrid electrode has more open electrode structure, which may have brought some benefits for electrolyte wetting and Li^+-ion transport.

By greatly minimizing the inactive electrode components such as the carbon black and polymeric binder, the hybrid GNSs/$Li_4Ti_5O_{12}$/SWCNTs electrode can maximize the energy density as seen in Figure 4c. At 1 C-rate, the hybrid electrode delivered 144.5 mA h g^{-1} while the pristine and bead-milled $Li_4Ti_5O_{12}$ electrodes showed 119.5 and 118.4 mA h g^{-1}, respectively. Here, the capacities were calculated based on the total electrode mass, not just with the mass of $Li_4Ti_5O_{12}$ for the specific capacity calculation. The difference was further pronounced at higher C-rates. For example, the GNSs/$Li_4Ti_5O_{12}$/SWCNTs electrode showed 126.3 mA h g^{-1} and the pristine and bead-milled $Li_4Ti_5O_{12}$ electrodes delivered 84.8 and 70.5 mA h g^{-1} at 20C, respectively. Thus, our hybrid electrode strategy has a significant advantage to secure high electrode energy density. The better rate capability of the pristine $Li_4Ti_5O_{12}$ electrode than that of the bead-milled $Li_4Ti_5O_{12}$ electrode is mainly due to better electrical contact with carbon black.

During the high C-rate test, an interesting voltage behavior was found in the pristine and bead-milled $Li_4Ti_5O_{12}$ electrodes. As presented in Figure 4d–e, the discharge (Li^+-insertion) average voltages of the GNSs/$Li_4Ti_5O_{12}$/SWCNTs hybrid electrode did not vary not-

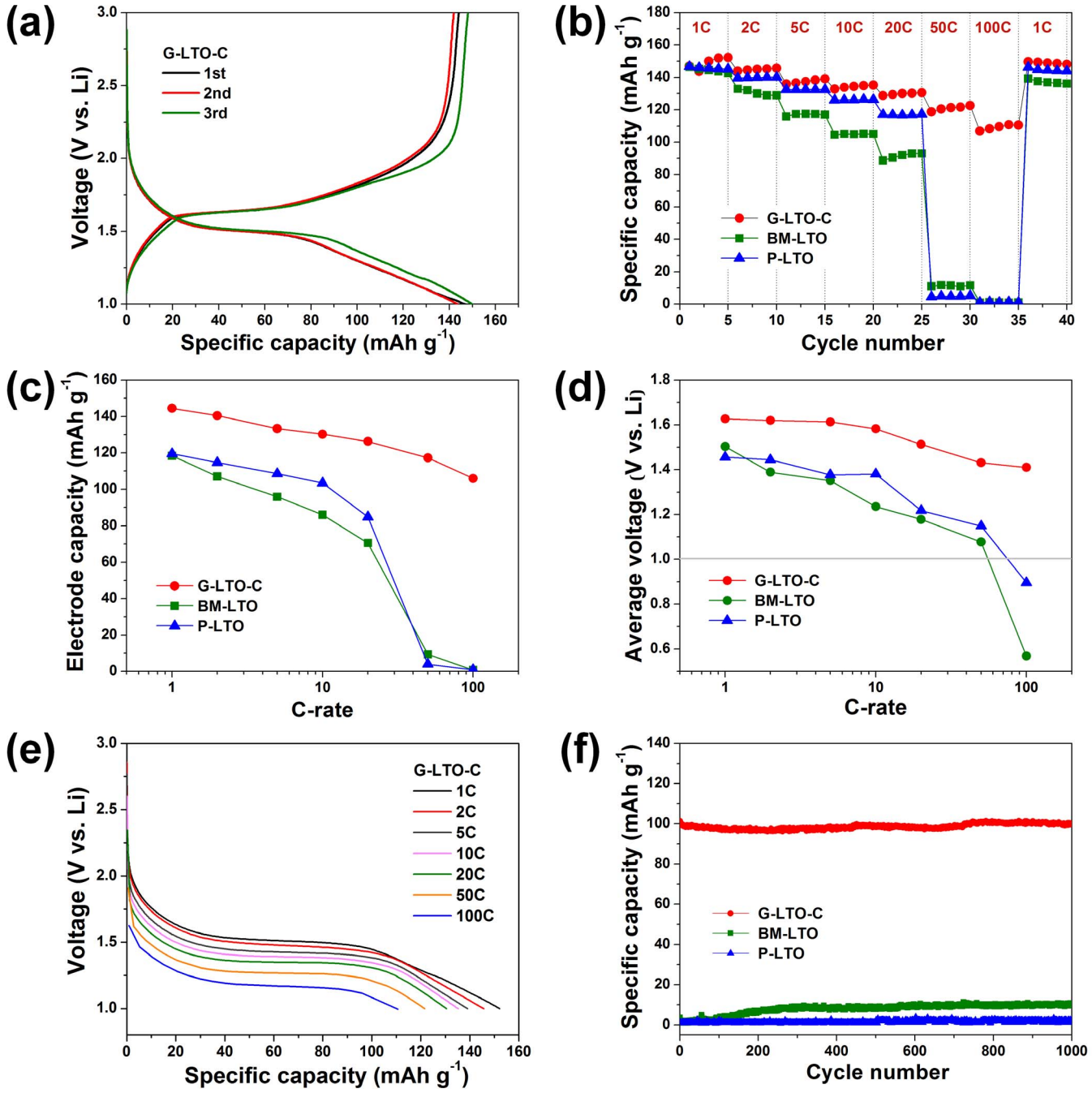

Figure 4 | Electrochemical characterizations of GNSs/$Li_4Ti_5O_{12}$/SWCNTs hybrid electrodes. (a) Galvanostatic charge/discharge voltage curves of the GNSs/$Li_4Ti_5O_{12}$/SWCNTs hybrid electrode (G-LTO-C; G-9 layer LTO-C) at 1 C-rate and room temperature, (b) discharge (Li-insertion) capacities of G-LTO-C, the pristine $Li_4Ti_5O_{12}$ electrode (P-LTO; 1.3 mg cm^{-2}), and the bead-milled $Li_4Ti_5O_{12}$ electrode (BM-LTO; 1.3 mg cm^{-2}) during cycling with different current densities, (c) electrode discharge capacities of G-LTO-C, P-LTO and BM-LTO, (d) average discharge voltages of G-LTO-C, P-LTO and BM-LTO, (e) discharge voltage curves of G-LTO-C at different C-rates, (f) cycle performance of G-LTO-C, P-LTO and BM-LTO at 100 C-rate for 1000 cycles.

ably during the rate-capability test. The lower average voltage (high polarization) of the slurry-casted $Li_4Ti_5O_{12}$ electrode will reduce the energy density of an electrochemical full cell. In particular, the slurry-casted electrodes raise an efficiency issue at the 100 C-rate charge/discharge. At this current density, as soon as the galvanostatic current was applied, the voltage dropped below 1.0 V vs. Li^+/Li, which induces the irreversible solid electrolyte interphase (SEI) layer formation by decomposition of the carbonate-based liquid electrolyte. Since $Li_4Ti_5O_{12}$ is considered as a very efficient anode material for the long-term and large-scale energy storage, the degradation of the coulombic efficiency is a significant issue.

Finally, to further investigate the cyclability and kinetic properties of the GNSs/$Li_4Ti_5O_{12}$/SWCNTs hybrid electrode, a long-term cycling test was carried out for 1000 cycles at an extremely high rate of 100C was. A capacity of 100 mA h g^{-1} maintained after 1000 cycles (Figure 4f). However, the both slurry-casted electrodes showed negligible capacities below 10 mA h g^{-1} during the 100 C-rate cycling; Supplementary Fig. S7c and S7d exhibit the cycle performance of the

GNSs/$Li_4Ti_5O_{12}$/SWCNTs electrodes and the slurry-casted electrodes, respectively. The long-term cycling performance confirms the mechanical stability of the hybrid electrode as well as the electrochemical reversibility.

In summary, we have proposed a novel electrode design strategy with the binder-free carbon network structure, which is very effective for the electrochemical utilization of the carbon-free nano-$Li_4Ti_5O_{12}$ particles. The new hybrid electrode composed of the self-aggregated nanoporous $Li_4Ti_5O_{12}$ spherical particles sandwiched between GNSs and SWCNTs networks was successfully fabricated via the E-spray and air-spray deposition processes. The total carbon content wrapping the $Li_4Ti_5O_{12}$ aggregates was minimized to 2.9 wt.% in the multi-stacked structure. The compact $Li_4Ti_5O_{12}$ aggregates provide good physical contacts between the carbon-free $Li_4Ti_5O_{12}$ nanoparticles and efficient electrolyte channels along the interparticle void space. The GNSs and SWCNTs networks interconnecting each $Li_4Ti_5O_{12}$ aggregate are effectively offering high electron transport pathways, leading to high rate capability as well as enhanced mechanical stability. With this hybrid electrode structure, we could maximize the electrode energy density (the electrode capacity of 100 mA h g^{-1} and the average voltage of 1.41 V at 100 C-rate) and maintain stable cycling capacities up to 1000 cycles even at the rate of 100C. Furthermore, our electrode fabrication process is facile, reproducible and efficient, so it could be easily applied to other nanostructured electrode materials with desirable morphologies.

Methods

Fabrication of multi-stacked GNSs/$Li_4Ti_5O_{12}$/SWCNTs hybrid electrodes. The fabrication procedure of the GNSs/$Li_4Ti_5O_{12}$/SWCNTs hybrid electrode consists of the following sequential steps: (1) bead-milling of $Li_4Ti_5O_{12}$ powder, (2) air-spraying of GNSs suspension, (3) electrostatic-spraying of bead-milled $Li_4Ti_5O_{12}$ suspension, and (4) air-spraying of SWCNTs suspension.

Bead-milling of $Li_4Ti_5O_{12}$ powder. The commercial $Li_4Ti_5O_{12}$ powder (<100 nm, <99%, Sigma–Aldrich Co., Ltd., USA) was mixed with ethanol in a weight ratio of 0.02 : 0.98. Then the mixture was dispersed for 30 min. under ultrasonic agitation. The $Li_4Ti_5O_{12}$ suspension was filled in the high energy ball milling vessel with the ZrO_2 beads media (Ø 0.1 mm in diameter; with a packing ratio of beads as high as ~85%) and the feeding pump to deliver the $Li_4Ti_5O_{12}$ dispersed solution (Supplementary Fig. S1). The $Li_4Ti_5O_{12}$ dispersed solution was then agitated by a shaft with arms, rotating at a high speed of ~4000 rpm for 60 min. Nano-sized $Li_4Ti_5O_{12}$ particles with an average diameter of 21 nm were obtained after filtration and drying. The crystal structures and particle size of the bead-milled $Li_4Ti_5O_{12}$ samples with different bead-milling time were analyzed by X-ray diffraction (XRD; RIGAKU, D/MAX-RC).

Air-spray of GNSs containing solution. Graphene nanosheets (GNSs, XGnP C-grade, XG Science Co., Ltd., USA; Supplementary Fig. S9a) dispersion in N, N dimethylformamide (DMF, 99.8%, Sigma–Aldrich Co., Ltd., USA) was prepared as shown in Supplementary Fig. S10a. GNSs (0.1 g) were first dissolved into the DMF (500 ml), and the suspended GNSs were uniformly dispersed by homogenizer with accumulated energy of 20 kJ. The dispersion solution was sprayed on a stainless steel foil using an air-spray gun connected to an air pump. The sprayed GNSs solution on the foil was dried to evaporate the DMF solvent. To evaporate the solvent quickly, the temperature of the substrate, which was attached with tape to the hot plate, was maintained at 160°C. The air-spraying and subsequent drying processes were repeated several times to ensure the uniform deposition of GNSs on the stainless steel foil.

E-spray of the bead-milled $Li_4Ti_5O_{12}$ containing solution. To prepare a starting solution, the nanosized $Li_4Ti_5O_{12}$ powder (1.25 g) obtained from step (1) was dispersed in ethanol (6 ml) and agitated for 1 h (Supplementary Fig. S10b). Next, the E-spray of the dispersion solution was carried out with a feeding rate of 20 μl min^{-1} on the GNSs-coated stainless steel foil that was vertically positioned at 20 cm away from the syringe needle (25 gauge) under a constant potential of 15 kV to collect self-aggregated nanoporous $Li_4Ti_5O_{12}$ spherical particles. The self-aggregated nanoporous $Li_4Ti_5O_{12}$ deposited on the GNSs were dried at 80°C for 2 h.

Air-spray of SWCNTs containing solution. SWCNTs (Purified SW-CNT, Unidym Co., Ltd., USA; Supplementary Fig. S9b) dispersed solution in DMF solvent was prepared with the same processing method as that of the GNSs solution in step (2) (Supplementary Fig. S10c). The dispersion solution was sprayed on a stainless steel foil using an air-spray gun connected to a vacuum pump. The sprayed SWCNTs solution on the GNSs/$Li_4Ti_5O_{12}$ was dried to evaporate the DMF solvent. To easily evaporate the solvent, the temperature of the SUS/GNSs/$Li_4Ti_5O_{12}$ substrate, which is attached with tape to the hot plate, was maintained at 160°C. The air-spraying and subsequent drying processes were repeated several times for uniform deposition of SWCNTs and dense interconnection with the substrate. The surface morphology of the samples was analyzed using a scanning electron microscope (SEM, Philips, XL30SFEG) and transmission electron microscope (TEM, FEI, Tecnai F30 S-Twin).

Electrochemical characterization. For comparison, the pristine and bead-milled $Li_4Ti_5O_{12}$ powders were mixed with Super-P carbon black and polyvinylidene fluoride (PVDF) in a weight ratio of 82 : 10 : 8 with n-methyl-2-pyrrolidone (NMP) as a dispersant. The mixed paste was casted on the Cu foil and subsequently dried at 100°C overnight. The electrochemical performances of the GNSs/$Li_4Ti_5O_{12}$/SWCNTs hybrid electrode and the two laminate electrodes were evaluated with coin half-cells (2032, Hohsen). A Li-metal foil was used as the counter electrode and 1 M $LiPF_6$ in an 1 : 1 mixture (by volume) of ethylene carbonate: diethylene carbonate (Soulbrain Co., Ltd., South Korea) was used as the electrolyte. The separator was a Celgard 2325 (25 μm thick). The cells were galvanostatically charged and discharged between 1.0 and 3.0 V at various current densities. All of the potentials refer to Li/Li^+. Electrochemical impedance spectroscopy (EIS) analysis (Biologic VSP-3 potentiostat) was conducted at different C-rates, and an AC perturbation of 10 mV was applied for a frequency sweep from 1 MHz to 200 mHz.

1. Goodenough, J. B. & Park, K. S. The Li-Ion Rechargeable Battery: A Perspective. *J. Am. Chem. Soc.* **135**, 1167–1176 (2013).
2. Etacheri, V., Marom, R., Elazari, R., Salitra, G. & Aurbach, D. Challenges in the development of advanced Li-ion batteries: a review. *Energy Environ. Sci.* **4**, 3243–3262 (2011).
3. Tarascon, J. M. & Armand, M. Issues and challenges facing rechargeable lithium batteries. *Nature* **414**, 359–367 (2001).
4. Song, Z. M. *et al.* Origami lithium-ion batteries. *Nat. Commun.* **5**: 3140 doi:10.1038/ncomms4140 (2014).
5. Hu, L. B., Wu, H., La Mantia, F., Yang, Y. A. & Cui, Y. Thin, Flexible Secondary Li-Ion Paper Batteries. *ACS Nano* **4**, 5843–5848 (2010).
6. Choi, K. H. *et al.* Thin, Deformable, and Safety-Reinforced Plastic Crystal Polymer Electrolytes for High-Performance Flexible Lithium-Ion Batteries. *Adv. Funct. Mater.* **24**, 44–52 (2014).
7. Liu, B. *et al.* Hierarchical silicon nanowires-carbon textiles matrix as a binder-free anode for high-performance advanced lithium-ion batteries. *Sci. Rep.* **3**, 1622; DOI: 10.1038/srep01622 (2013).
8. Bruce, P. G., Scrosati, B. & Tarascon, J. M. Nanomaterials for rechargeable lithium batteries. *Angew. Chem. Int. Ed.* **47**, 2930–2946 (2008).
9. Zhang, H. X. *et al.* Cross-Stacked Carbon Nanotube Sheets Uniformly Loaded with SnO_2 Nanoparticles: A Novel Binder-Free and High-Capacity Anode Material for Lithium-Ion Batteries. *Adv. Mater.* **21**, 2299–2304 (2009).
10. Sun, Y. M. *et al.* Morphosynthesis of a hierarchical MoO_2 nanoarchitecture as a binder-free anode for lithium-ion batteries. *Energy Environ. Sci.* **4**, 2870–2877 (2011).
11. Kim, J. H., Nam, K. W., Ma, S. B. & Kim, K. B. Fabrication and electrochemical properties of carbon nanotube film electrodes. *Carbon* **44**, 1963–1968 (2006).
12. Park, K. S., Schougaard, S. B. & Goodenough, J. B. Conducting-polymer/iron-redox-couple composite cathodes for lithium secondary batteries. *Adv. Mater.* **19**, 848–851 (2007).
13. Ohzuku, T., Ueda, A. & Yamamoto, N. Zero-Strain Insertion Material of $Li[Li_{1/3}Ti_{5/3}]O_4$ for Rechargeable Lithium Cells. *J. Electrochem. Soc.* **142**, 1431–1435 (1995).
14. Amatucci, G. G., Badway, F., Du Pasquier, A. & Zheng, T. An asymmetric hybrid nonaqueous energy storage cell. *J. Electrochem. Soc.* **148**, A930–A939 (2001).
15. Ronci, F. *et al.* High-resolution in-situ structural measurements of the $Li_{4/3}Ti_{5/3}O_4$ "Zero-Strain" insertion material. *J. Phys. Chem. B* **106**, 3082–3086 (2002).
16. Amine, K. *et al.* Nanostructured Anode Material for High-Power Battery System in Electric Vehicles. *Adv. Mater.* **22**, 3052–3057 (2010).
17. He, Y. B. *et al.* Gassing in $Li_4Ti_5O_{12}$-based batteries and its remedy. *Sci. Rep.* **2**, 913; DOI:10.1038/srep00913 (2012).
18. Wang, F. *et al.* Excess lithium storage and charge compensation in nanoscale $Li_{4+x}Ti_5O_{12}$. *Nanotechnology* **24**, 424006; DOI:10.1088/0957-4484/24/42/424006 (2013).
19. Song, M. S., Benayad, A., Choi, Y. M. & Park, K. S. Does $Li_4Ti_5O_{12}$ need carbon in lithium ion batteries? Carbon-free electrode with exceptionally high electrode capacity. *Chem. Commun.* **48**, 516–518 (2012).
20. Kim, C., Norberg, N. S., Alexander, C. T., Kostecki, R. & Cabana, J. Mechanism of Phase Propagation During Lithiation in Carbon-Free $Li_4Ti_5O_{12}$ Battery Electrodes. *Adv. Funct. Mater.* **23**, 1214–1222 (2013).
21. Park, K. S., Benayad, A., Kang, D. J. & Doo, S. G. Nitridation-Driven Conductive $Li_4Ti_5O_{12}$ for Lithium Ion Batteries. *J. Am. Chem. Soc.* **130**, 14930–14931 (2008).
22. Yi, T. F. *et al.* Recent development and application of $Li_4Ti_5O_{12}$ as anode material of lithium ion battery. *J. Phys. Chem. Solids* **71**, 1236–1242 (2010).
23. Chen, C. H., Kelder, E. M. & Schoonman, J. Electrostatic sol-spray deposition (ESSD) and characterisation of nanostructured TiO_2 thin films. *Thin Solid Films* **342**, 35–41 (1999).
24. Modesto-Lopez, L. B. & Biswas, P. Role of the effective electrical conductivity of nanosuspensions in the generation of TiO_2 agglomerates with electrospray. *J. Aerosol Sci.* **41**, 790–804 (2010).

25. Hogan, C. J. & Biswas, P. Porous film deposition by electrohydrodynamic atomization of nanoparticle sols. *Aerosol Sci. Tech.* **42**, 75–85 (2008).
26. Hwang, D. *et al.* Electrospray Preparation of Hierarchically-structured Mesoporous TiO_2 Spheres for Use in Highly Efficient Dye-Sensitized Solar Cells. *ACS Appl. Mater. Inter.* **3**, 2719–2725 (2011).
27. Sorensen, E. M. *et al.* Three-dimensionally ordered macroporous $Li_4Ti_5O_{12}$: Effect of wall structure on electrochemical properties. *Chem. Mater.* **18**, 482–489 (2006).
28. Zhu, G. N. *et al.* Carbon-coated nano-sized $Li_4Ti_5O_{12}$ nanoporous micro-sphere as anode material for high-rate lithium-ion batteries. *Energy Environ. Sci.* **4**, 4016–4022 (2011).
29. Qian, J. F., Zhou, M., Cao, Y. L., Ai, X. P. & Yang, H. X. Template-Free Hydrothermal Synthesis of Nanoembossed Mesoporous $LiFePO_4$ Microspheres for High-Performance Lithium-Ion Batteries. *J. Phys. Chem. C* **114**, 3477–3482 (2010).
30. Bolotin, K. I. *et al.* Ultrahigh electron mobility in suspended graphene. *Solid State Commun.* **146**, 351–355 (2008).
31. Lee, C., Wei, X. D., Kysar, J. W. & Hone, J. Measurement of the elastic properties and intrinsic strength of monolayer graphene. *Science* **321**, 385–388 (2008).
32. Koenig, S. P., Boddeti, N. G., Dunn, M. L. & Bunch, J. S. Ultrastrong adhesion of graphene membranes. *Nat. Nanotechnol.* **6**, 543–546 (2011).
33. Kan, J. & Wang, Y. Large and fast reversible Li-ion storages in Fe_2O_3-graphene sheet-on-sheet sandwich-like nanocomposites. *Sci. Rep.* **3**, 3502 DOI: 10.1038/srep03502 (2013).
34. Wang, D. H. *et al.* Self-Assembled TiO_2-Graphene Hybrid Nanostructures for Enhanced Li-Ion Insertion. *ACS Nano* **3**, 907–914 (2009).
35. Vinayan, B. P. *et al.* Synthesis of graphene-multiwalled carbon nanotubes hybrid nanostructure by strengthened electrostatic interaction and its lithium ion battery application. *J. Mater. Chem.* **22**, 9949–9956 (2012).
36. Wang, W. & Kumta, P. N. Nanostructured Hybrid Silicon/Carbon Nanotube Heterostructures: Reversible High-Capacity Lithium-Ion Anodes. *ACS Nano* **4**, 2233–2241 (2010).
37. Shen, L. F. *et al.* In situ growth of $Li_4Ti_5O_{12}$ on multi-walled carbon nanotubes: novel coaxial nanocables for high rate lithium ion batteries. *J. Mater. Chem.* **21**, 761–767 (2011).
38. Qiu, J. Y., Hotta, Y., Sato, K., Watari, K. & Mitsuishi, K. Fabrication of fine AlN particles by pulverizing with very small ZrO_2 beads. *J. Am. Ceram. Soc.* **88**, 1676–1679 (2005).
39. Dylla, A. G., Xiao, P. H., Henkelman, G. & Stevenson, K. J. Morphological Dependence of Lithium Insertion in Nanocrystalline TiO_2(B) Nanoparticles and Nanosheets. *J. Phys. Chem. Lett.* **3**, 2015–2019 (2012).
40. Meethong, N., Kao, Y. H., Carter, W. C. & Chiang, Y. M. Comparative Study of Lithium Transport Kinetics in Olivine Cathodes for Li-ion Batteries. *Chem. Mater.* **22**, 1088–1097 (2010).

Acknowledgments

This work was supported by the KIMM and the National Research Council of Science & Technology (NST), Republic of Korea.

Author contributions

J.-H.C., W.-H.R., K.P. and I.-D.K. designed and carried out research, analyzed data and wrote the paper. J.-D.J., S.-M.J. and D.-S.L. discussed the results. All authors contributed research and reviewed the manuscript.

Additional information

Supplementary information accompanies this paper at http://www.nature.com/scientificreports

Competing financial interests: The authors declare no competing financial interests.

How to cite this article: Choi, J.-H. *et al.* Multi-layer electrode with nano-$Li_4Ti_5O_{12}$ aggregates sandwiched between carbon nanotube and graphene networks for high power Li-ion batteries. *Sci. Rep.* **4**, 7334; DOI:10.1038/srep07334 (2014).